Cofiring of hydrogen and pulverized coal in rotary kilns using one integrated burner

Citation for the original published paper (version of record):
Johansson, A., Fernberg, J., Sepman, A. et al (2024). Cofiring of hydrogen and pulverized coal in rotary kilns using one integrated burner. International Journal of Hydrogen Energy, 90: 342-352.
http://dx.doi.org/10.1016/j.ijhydene.2024.09.327

(article starts on next page)

International Journal of Hydrogen Energy 90 (2024) 342–352

Contents lists available at ScienceDirect

International Journal of Hydrogen Energy

journal homepage: www.elsevier.com/locate/he

Cofiring of hydrogen and pulverized coal in rotary kilns using one integrated burner

Andreas Johansson [a,*], Johannes Fernberg [a], Alexey Sepman [a], Samuel Colin [b], Jonas Wennebro [a], Fredrik Normann [b], Henrik Wiinikka [a,c]

[a] RISE AB, 94128, Piteå, Sweden
[b] Department of Energy Technology, Chalmers University of Technology, 41296, Gothenburg, Sweden
[c] Division of Energy Engineering, Luleå University of Technology, 97187, Luleå, Sweden

ARTICLE INFO

Handling Editor: Umit Demirci

Keywords:
Hydrogen combustion
Coal combustion
Cofiring
Rotary kiln
Emissions

ABSTRACT

The grate-kiln process for iron-ore pellet induration utilizes pulverized coal fired burners. In a developed infrastructure for H_2, it might be desirable to heat the existing rotary kilns with renewably produced H_2. Technical challenges of H_2 heating of grate-kilns include high emissions of NO_X and maintaining sufficient heat transfer to the pellet bed. This article examined cofiring (70% coal/30% H_2) in 130 kW experiments using two different integrated burner concepts. Compared to pure coal combustion, cofiring creates a more intense, smaller flame with earlier ignition and less fluctuations. The process temperature and heat transfer are enhanced in the beginning of the kiln. The co-fired flames emit 32% and 78% less NO_X emissions compared to pure coal and H_2 combustion, respectively. We can affect the combustion behavior and NO_X emissions by the burner design. H_2/coal cofiring using integrated burners is probably an attractive solution for emission minimization in rotary kilns.

1. Introduction

Rotary kilns are used to heat solid materials to high temperatures (>1000 °C) in a continuous process, for example in cement-, pulp and paper-, and iron ore industries [1–4]. The cement industry alone contributes to ~5% of global greenhouse gas (GHG) emissions whereas the iron and steel industry emits ~7% of global GHG emissions [5,6]. Roughly half of the total CO_2 emitted from the cement industry is from combustion of fossil fuels in the rotary kilns used for calcination and clinker formation; the remaining is emitted from the calcination of the limestone [5]. In the iron and steel industry, combustion in kilns is used in the sintering process of iron ore pellets inside the so-called grate-kiln (GK) induration process [7]. Consequently, rotary kiln operators must heavily reduce the fossil fuel usage in their furnaces to be able to reach the 1.5 °C global temperature increase target, signed by 196 parties in the 2015 Paris agreement [8] and the related targets by the European Union to reduce CO_2 emissions by 55% by 2030 (relative to 1990) and become climate neutral by 2050 [9].

According to Julian [10], carbon neutral iron-ore induration processes, for the iron and steel industry, should be developed promptly. Pelletizing plants will be in operation for a foreseeable future, therefore, retrofittable solutions for reducing their emissions are essential. In Europe, focus is on electrification and hydrogen-based steelmaking [10]. In a developed infrastructure for H_2, it may be desirable to apply H_2 also for heating of the grate kiln induration process.

Replacing a fraction of the coal fuel in the kiln with H_2 gas from renewable powered water electrolysis will reduce the CO_2 emissions proportionally to the mixing ratio of the fuels. To our best knowledge no investigations of H_2 and coal cofiring in a single integrated burner sharing a single flame is reported in the literature. A challenge with H_2 combustion in grate kilns is high NO_X emissions [11,12]. Anthropogenic NO_x causes atmospheric ozone depletion, smog clouds, and acid rainfall [13]. Pure H_2 flames typically produce a larger amount of NO_X compared to fossil oils and coal due to the higher flame temperatures [14,15]. A high flame temperature allows the N_2 in the combustion air to form NO_X via the well-known Zeldovich mechanism [16]. By design, GK induration plants operate at large air-to-fuel equivalence ratio (λ), typically in the range of 4–6, for plants designed to oxidize magnetite (Fe_3O_4) to hematite (Fe_2O_3). The secondary combustion air in the process is preheated to temperatures above 1000 °C [17]. The large amount of excess secondary air required in the process along with the construction of the rotating kiln make it difficult to apply conventional

* Corresponding author.
E-mail address: andreas.h.johansson@ri.se (A. Johansson).

https://doi.org/10.1016/j.ijhydene.2024.09.327
Received 30 May 2024; Received in revised form 9 September 2024; Accepted 23 September 2024
Available online 5 October 2024

primary NO_X mitigation strategies such as staged combustion [12]. Another potential obstacle with H_2 combustion in kilns is that the flame does not contain any radiating solid particles (i.e., soot, char and fly ash). It has previously been shown that radiation from the flame dominates the heat flux to the wall during coal combustion in the kiln [11, 18]. The potential change in radiation properties and shape of H_2 flames can potentially reduce heat transferred to the pellet bed affecting the production rate, quality of the product, and furnace efficiency negatively.

NO_X formation and heat transfer from combustion of solid and gaseous fuels have been studied extensively, see for example [16,19,20]. Furthermore, there are also studies of cofiring solid and gaseous fuels, where some of the investigations also involves H_2 [21–25]. However, all these studies applied a separate flame for each fuel, and with focus on other technical applications than rotary kilns. Pisa et al. [21] experimentally studied the influence of hydrogen enriched gas (HRG). HRG was premixed with primary air and pulverized brown coal in a burner installed in a 2 MW pilot furnace. They found that SO_2 emissions decreased while NO_X emission was increased with the addition of HRG in the primary air. Kim et al. [26] developed a CFD model of a 550 MW tangentially fired pulverized coal boiler co-fired with CH_4 in a second combustion stage. They found that introducing CH_4 up to 40% of total power in a secondary combustion zone decreased the predicted NO_X emissions by up to 70%. The decrease in NO_X pollution is explained by less production of fuel NO_X due to a lower flow of coal and by NO_X reburning in the CH_4 combustion zone. Since CH_4 contains carbon atoms, the reduction of CO_2 emissions was not severe. The amount of unburned fuel was reduced when the CH_4/coal ratio was increased.

There are several recent studies on co-firing of coal and NH_3 [27–32]. NH_3 is a H_2 rich chemical with promising properties as a renewable H_2 carrier that is combustible directly without requiring a H_2 extraction process [33]. Although NH_3 is H_2 rich, the physical properties of the chemical and its combustion behavior differs from pure H_2 combustion [29]. Aoyang et al. investigated co-firing of 0–50% NH_3 (on power basis) and pulverized coal in a drop tube furnace [27]. The authors found that co-firing with NH_3 increases the NO_x emissions and drastically reduces the SO_2 flue gas emissions compared to pulverized coal combustion. Co-firing of NH_3 leads to higher concentrations of submicron particles [27]. Tamura et al. studied co-firing of coal and NH_3 in a 1.2 MW bench scale burner [32]. Experiments were performed with a small amount of excess oxygen O_2 <5% with air staging technology to reduce NO_x emissions. The NH_3 was injected differently into the process, either premixed with coal, into the coal burner or separately at the side wall. Side wall injection increases the NO_X emissions while the NO_X emissions using premixed and burner gun injection remained at the same level as coal for mixing ratios between 0 and 30% NH_3 on energy basis. However, further increase of NH_3/coal blending ratio results in increased NO_x emissions. The amount of unburned carbon decrease also as the mixing ratio of NH_3 increased.

In this work, we study cofiring of 30% (energy basis) H_2 and non-premixed pulverized coal in a pilot scale furnace (130 kW) designed to simulate the combustion process inside rotary kilns [11]. The combustion characteristics of H_2/coal cofiring is compared to pure pulverized coal and pure H_2 combustion. Two burner concepts are investigated: i) an annular H_2 injection around a central coal injection and ii) an annular coal injection around a central H_2 injection. Moreover, several H_2 injection velocities are investigated in both burner concepts. The effect of H_2/coal cofiring on NO_X emissions and heat transfer relevant for rotary kiln applications are discussed.

2. Experimental conditions

2.1. Experimental setup

This study was performed in the test furnace called the horizontal industrial combustion kiln (HICK) located at RISE in Piteå, Sweden. The HICK, which has a maximum fuel capacity of 150 kW, is a pilot-scale facility designed to simulate combustion conditions inside different types of rotary kilns. A sketch of the HICK with the system components and the location of the measurement ports are shown in Fig. 1. The HICK consists of six main parts: the fuel injection system, the burner hood, the kiln, the transfer chute, the boiler, and the flue gas channel.

Each fuel has a dedicated fuel feeding system. H_2 is supplied from a pressurized packages of 24 tubes (50 dm^3 each at 200 bar pressure) located outside the building. The pressure in the gas transporting pipe was decreased by a pressure regulator to ~12 bar. The feeding rate of H_2 to the burner was regulated by a *Bronkhorst* (EL-*FLOW Select F*-203 A V) mass flow controller (MFC). The pulverized coal was supplied from a 0.6 m^3 fuel hopper placed on top of weight cells for coal mass flow rate measurements. The coal feeding system dispatched the coal trough screw feeding into a fuel shaft for further transportation with transport air to the burner. The mass flow of coal was controlled by the rotation speed of the screws. Transport air was fed (trough an ejector) to the fuel shaft by an MFC (Red-y, GSC-D5SS-BB13). Burner air was fed to the burner separately through a pipe controlled with a separate MFC (Brooks, SLA5800 Series).

The burner hood consists of a burner unit and a preheating unit (denoted 3 and 4 in Fig. 1). In commercial induration plants, the combustion air is preheated by waste heat to increase the efficiency of the system [34]. To mimic this, the HICK has a preheating system consisting of eight 15 kW air heaters (Leister, LE 10 000 H T) with a maximum capacity of 20 dm^3/s that preheats the air to ~850 °C based on *S*-type fine wire thermocouple measurements. The preheated secondary air is separated vertically in two rows by a horizontal plate containing the burner.

Two conceptual burner designs with several configurations each were used, see the nozzles sketched in Fig. 2 and drawings of the burners are presented in Fig. S1 in the supplementary material. In burners denoted O-, coal is feed through the central pipe and H_2 through an annular pipe with a plate with 1–8 holes with a diameter of 2 mm. In burners denoted I-, H_2 was injected through the central pipe through an opening with a diameter of 2–6 mm, while coal was feed through the annular pipe. A primary air register without swirl provides combustion air for ignition and cooling of the burner tip in both burner concepts. The burner tip is inserted 150 mm into the kiln section (see x-axis in Fig. 1).

The brick lined horizontal furnace has a length of 3300 mm and has a square shaped cross section with an inner height and width of 550 mm. The process temperature (T_{proc}) is measured with six thermocouples (type K, 3 mm) located along the roof of the kiln. The thermocouples barely penetrate the insulation, a few millimeters into the gas stream. The kiln has several access ports for measurements. Most relevant to this study are three optical ports (P2, P4, and P5) and two ordinary measurement ports suitable for probe measurements (P1 and P3), see Fig. 1. P2 and P4 are located on the front side of the kiln at 970 mm and 2500 mm from the start of the kiln respectively. P5 is located at the back of the kiln, opposite the front of the burner and the hood. P1 and P3 are also on the front side of the kiln at 720 mm and 2000 mm from the beginning of the kiln.

The kiln gradually reduces at the end into the smaller 230 mm square shaped transfer chute that connects the kiln to the boiler. The T_{proc} of the transfer chute was measured with a 1.5 mm K-type thermocouple located in the center line of the transfer chute.

In the boiler, the flue gas is cooled down to ~400 °C. The HICK was operated at a sub-atmospheric pressure of ~15 Pa regulated by a flue gas fan in the exhaust gas system. There are small ports in the beginning of the chimney, located approximately 500 mm after the boiler outlet. These ports provide access for gas measurements of the flue gas composition.

2.2. Measurement equipment

The wet flue gas composition in the chimney was continuously

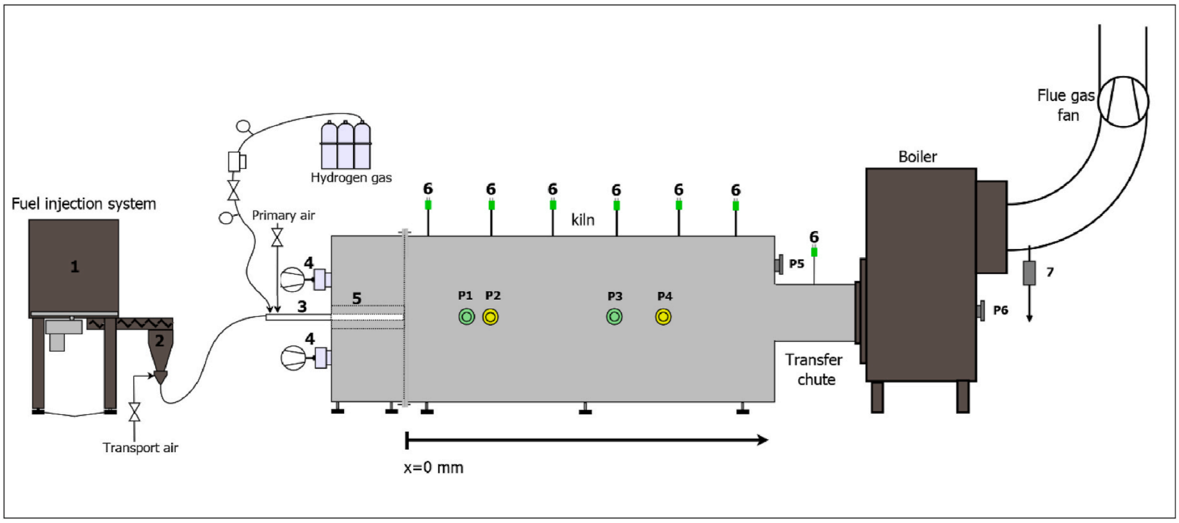

Fig. 1. The HICK and the experimental setup; (1) Fuel silo; (2) Fuel transport shaft; (3) Burner; (4) Preheated secondary air fans; (5) Burner hood; (6) Thermocouples; (7) Filtered flue gas access. The different measurement port P1–P6 are also shown in the Figure. P1 and P3 are used for heat transfer measurements. P2 and P4 are used for Tunable diode laser absorption measurements and emission measurements. The flame is video recorded through P5 and P6.

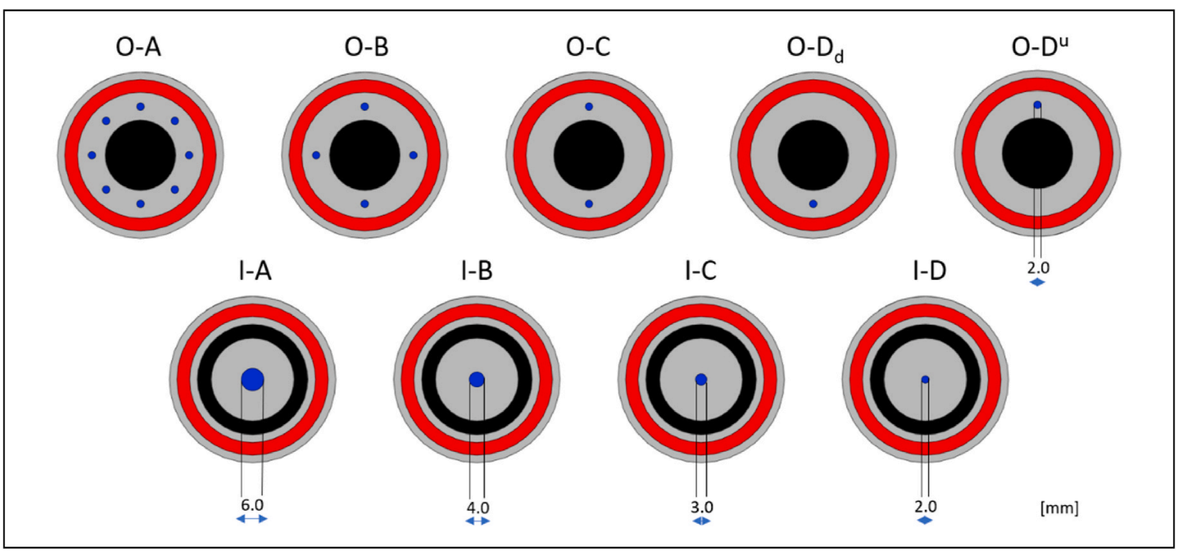

Fig. 2. Sketch of tested burner types, viewed from inside the kiln. Red areas represent primary air slit, the blue areas represent H_2 gas injection, and the black areas represents the coal injection. In burners O-, coal is injected centrally surrounded by H_2 injection holes and an annular primary air slit. In burners I-, H_2 is injected centrally with coal and primary air in annular slits surrounding the hydrogen injection. (For interpretation of the references to color in this figure legend, the reader is referred to the Web version of this article.)

measured with respect to H_2O, CO_2, CO, NO and NO_2 with a Fourier transform infrared spectrometer (MKS Multigas 2030 FTIR). In addition, the dry flue gas composition with respect to O_2, CO_2, CO, NO and NO_2 was measured with a flue gas analyzer using NDIR (non-dispersive infrared spectroscopy) in combination with a paramagnetic cell for O_2 with a traditional gas instrument (MRU Air MGA Prime). A heated filter filled with glass wool was used to remove particles in the gas drawn to the FTIR and MGA Prime. The gas was pumped to the instruments through a heated sampling line to prevent condensation, see (7) in Fig. 1. The gas composition for all combustion species except O_2 was determined using FTIR. The presented O_2 was measured with MGA Prime and then adjusted to wet basis using the FTIR-measured H_2O concentration. The heat transfer to the furnace wall was measured using an IFRF total heat flux probe that capture the total heat flux to a metal surface. Measurements were performed in ports P1 and P3 (see Fig. 1). The probe tip was aligned with the inner wall of the furnace and the measurements were performed for 15 min or until a stable value was attained. Detailed information on the total heat flux radiometer can be found in Ref. [35].

Videos of the flames were filmed through port 5 using a Samsung S22 S901B smartphone at a 1080 × 1920 resolution. No manual editing of the footage was performed except for cropping and trimming. Tunable diode laser absorption spectroscopy (TDLAS) and emission measurements were performed through ports P2 and P4 in Fig. 1.

2.3. Spectroscopic measurements

The gas temperature (T_{gas}) and H_2O concentration were measured using a TDLAS system which consists of a Nanoplus distributed feedback laser diode generating light at approximately 1.4 μm, a controller (Thorlabs, ITC4001), a photodetector (Thorlabs, PDA10) and a data acquisition system (National Instruments, with NI PXIe-6356 card). A more detailed description of the laser system, the procedure for data treatment, and sensor application examples can be found elsewhere [36–38]. The overall uncertainties in HICK TDLAS measurements were 75 °C and 15% (relative) for temperature and H_2O concentration. Emission spectra were measured using an Ocean Optics spectrometer (HR2000 + GC, HC-1 Grating, 600 gr/mm, blazed @ 300 nm) in the wavelength range from 200 nm to 1100 nm. The spectrometer was intensity-calibrated using a blackbody calibration source (Dias, PYROTHERM CS 1500). The radiation was collected by collimating lens (f = 8 mm) which focused the radiation into an optical fiber (with 400 μm core diameter) coupled with the spectrometer. The temperature of the particles in the flame ($T_{particle}$) was estimated by fitting the recorded spectra with a Planck function, for a more detailed description of the procedure see Ref. [11]. When the dominating radiation was the furnace wall, the wall temperature (T_{wall}) was determined.

2.4. Fuel analysis

Coal powder and H_2 were used as fuel in this study. The ultimate and proximate analysis as well as the particle size distribution of the coal can be seen in Table 1. The analysis also contains the relative uncertainties and references to the methods used to acquire the fuel analysis. The H_2 used in this study had a purity > 99.9 vol-%.

2.5. Experimental conditions

Preheating started with a 100-kW side mounted diesel burner installed in port P1 for about 18 h, followed by 2 h of heating with a 175 kW centrally mounted diesel burner. During central heating, the air preheating system was engaged to achieve a temperature profile in the furnace similar to the experimental kiln conditions. Finally, about an hour of pure coal combustion was performed to further heat the kiln to a stable temperature profile. After preheating the kiln, the integrated H_2/coal burner was installed. Between testing of different burners, a sequence of pure coal combustion was performed to avoid heat loss. Each burner configuration was tested until stable readings on the gas measurement instruments had been attained and heat transfer measurements had been performed, taking about 40–60 min per configuration. During cofiring the kiln was operated at 130 ± 1 kW with H_2 accounting for 32% of the power (~41 kW) and coal for the remaining 68% (~89 kW). Combustion was performed at a stochiometric ratio of approximately λ = 3.6, that is with an air flow of 6.66 nl/s going through the burner primary air register and a sum of 6400 dm^3/s through the eight electric air preheaters. The primary air used to transport the coal was 2.50 dm^3/s when cofiring and 3.33 dm^3/s for coal combustion. The operational conditions during the experiments are detailed in Table 2. The coal feeding rate is calculated from fuel silo weight measurements during operation. The actual secondary air flow rate and the resulting stochiometric ratio is calculated from the gas composition measured in the chimney (7 in Fig. 1).

Table 1
Coal fuel analysis.

	Unit	Measure	Analysis method
Particle size distribution			
<1 μm	%	2.1	Sieve
<5 μm	%	15.6	Sieve
<10 μm	%	29.2	Sieve
<15 μm	%	39.5	Sieve
<20 μm	%	47.6	Sieve
<45 μm	%	71.7	Sieve
<63 μm	%	81.3	Sieve
<90 μm	%	89.8	Sieve
<125 μm	%	95.2	Sieve
<180 μm	%	98.5	Sieve
<250 μm	%	99.6	Sieve
Proximate analysis (as received)			
Moisture	%	0.5 ± 0.05	ISO 589:2018 mod
Volatile matter	%	19.2 ± 1	ISO 562:2010 mod
Fixed carbon[a]	%	68.2 ± 5	ISO 562:2010 mod[a]
Ash	%	12.1 ± 0.6	ISO 1171:2018
Ultimate analysis (as received)			
Cl	%	<0.01	ASTM D4208-2019 mod
S	%	0.3	ASTM D4239-2018
C	%	77.0	ASTM-D5373:2016
H	%	3.9	ASTM-D5373:2016
N	%	1.33	ASTM-D5373:2016
O[a]	%	5.3	ASTM D3176-2015[a]
Calometric analysis (as received)			
LHV	MJ/kg	30.473	ISO 1928:2020

[a] Denotes calculated values.

3. Results and discussions

3.1. Flame characteristics

Video recordings of the flames (supplementary video 1 and video 2) illustrates the differences in flame characteristics of H_2/coal cofiring compared to pure coal and pure H_2 combustion. Representative snapshots of the flames extracted from the videos are presented in Figs. 3 and 4. We strongly encourage the reader to watch the videos in the supplementary material for an illustration of the dynamic combustion process. In general, the flames are centrally located in the furnace. Independent of burner configuration, the coal flame (Fig. 3a and 4a and video 1 and 2) is less bright and noticeably less compact compared to the H_2/coal cofiring flames (Fig. 3c and 4c and video 1 and 2). On short time scales (<1 s) the coal flame flickers due to turbulence. On larger time scales (>1 s) the overall intensity and point of ignition varied significantly resulting in a back and forward pulsating flame (see Video 1 and 2). This is due a variation in the fuel feeding rate, as observed previously during coal and biomass combustion in the HICK [11]. The pure H_2 flame is visible as a blue flame in the central part of the furnace (Fig. 3b and 4b). Recent findings suggest the blue emission comes from the radiative recombination of H + OH and OH + OH [39]. As seen here, the blue emission is so strong that it makes the H_2 flame visible although there is other black body radiation from the hot walls of the furnace that interferes in the visible spectrum of the light.

Compared to pure coal combustion, the H_2/coal cofiring resulted in a more compact and brighter flame that is more constant in flame size and with a higher flickering frequency (see Fig. 3c and 4c), probably due to higher turbulence combustion intensity from the H_2 jets in the burner. At the same time the pulsation of the flame is reduced. This observation suggests an earlier and more consistent ignition of the coal particles in the H_2/coal flame. Probably, the heat generated from H_2 combustion by the easily ignited H_2 injected into the coal particle stream serves both as a heat source for devolatilization of the coal particles and stable ignition source of the devolatilized gas. This have been previously observed for co-combustion of natural gas and coal powder flames [40]. As a result, the ignition and combustion of coal particles occurs closer to the burner, and pulsation is reduced.

Comparing the cofired burner designs (Fig. 3c–g and 4c to 4f), the burners with higher H_2 injection velocity give a high frequence flickering and brighter flame with a lower cross-sectional area covering less of the view from the porthole. This indicates that higher H_2 injection velocities produce compacter (in radial direction) and more intense flame at the centerline of the furnace. This could be a result of an increased entrainment of the preheated surrounding air into the flame, caused by the higher momentum of the H_2 jets in the burner which in turn increase the turbulence intensity and mixing of air and fuel in the jet flames, generating higher combustion intensity along the center line of the furnace.

The time resolved TDLAS measurements from port P2 and P4 for all burner cases are presented in Fig. 5 for T_{gas} and Fig. 6 for H_2O below. Tabulated average data and standard deviations from the TDLAS measurements are available in Tables S1 and S2. During coal combustion

Table 2
Operational conditions during experiments.

Burner	H_2		Coal		H_2 + Coal								
	O-A	I-A	O-A	I-A	O-A	*O*–B	*O*–C	*O*-D_d	*O*-D^u	I-A	I–B	I–C	I-D
H_2 Velocity [m/s]	517	460	–	–	155	310	620	1241	1241	138	310	552	1241
Power [kW]	139 ± 0		128 ± 2		130 ± 1								
Power H_2 [kW]	139		0		41								
Power coal [kW]	0		128 ± 2		89 ± 1								
Feeding rate coal [kg/h]	0		15.1 ± 0.2		10.5 ± 0.1								
Transport air flow rate [dm^3/s]	0		3.33		2.50								
Transport air temp [°C]	–		20		20								
Transport air velocity [m/s]	0		11.7		8.8								
Primary air flow rate [dm^3/s]	6.67		6.67		6.67								
Primary air temp [°C]	20		20		20								
Preheated Secondary air [dm^3/s]	106 ± 2		106 ± 2		106 ± 2								
Lambda	3.59 ± 0		3.56 ± 0.05		3.60 ± 0.03								

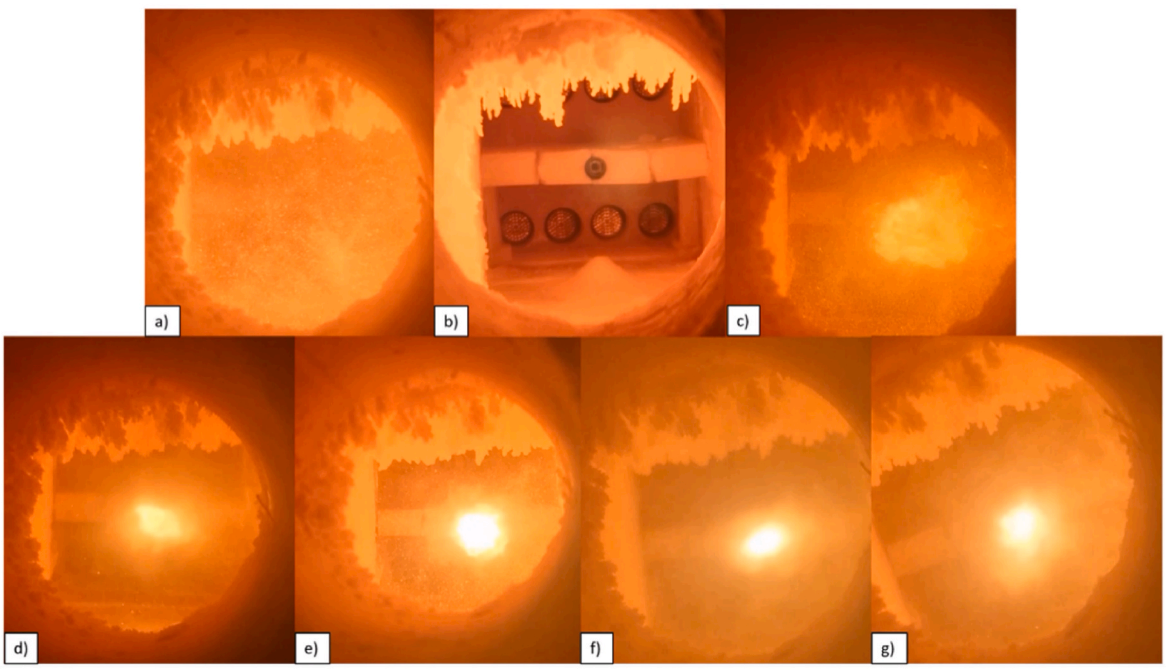

Fig. 3. Snapshots of the inside of the furnace when firing with hydrogen in the outer register. Coal combustion with burner O-A is shown in (a), H_2 combustion with burner O-A is shown (b), and co-fired combustion are shown in (*c*–g) with burner O-A in (c), burner *O*–B in (d), burner *O*–C in (e), burner *O*-D_d in (f) and burner *O*-D^u in (g).

there was a ~350 °C increase in T_{gas} (Fig. 5a and b) between port P2 and port P4 as well as an ~100% increase in H_2O concentration on average (Fig. 6a and b), indicating that a significant amount of the coal combustion occurs downstream of port P2. There are also large fluctuations in T_{gas} and the H_2O concentration in both P2 and P4 measurement positions (standard deviations 63 °C, 48 °C, 0.2% and 0.3%, respectively) indicates fluctuating combustion, which is in line with the flame observations. We did not evaluate the TDLAS measurements performed at P2 during pure H_2 combustions, since we expect temperatures well above 2000 °C at the center of the jet as well as sharp gradients of both T_{gas} and H_2O along the line of measurement, which makes the values unrepresentative of path-averaged temperatures and concentrations [41]. Therefore, only results from port 4 are presented in the figures for H_2 flames. Compared to pure coal combustion, the pure H_2 combustion conditions show almost no variations indicating almost constant combustion conditions and a stable flame. The average standard deviations of the temperature and H_2O concentration during pure H_2 combustion at P4 were 16 °C and 0.1%. Note that the average water concentration was 14.6 vol-% during pure H_2 combustion.

During H_2/coal cofiring, the average T_{gas} was on average 360 °C higher at P2 but slightly (50 °C) lower at P4 (Fig. 5e and f) relative to pure coal combustion, which suggests earlier ignition and a shorter flame for the cofiring cases. Furthermore, the fluctuations in T_{gas} and H_2O concentration are significantly lower than during coal combustion at both ports, although not as low as during H_2 combustion (at P4), which supports the previous statement that H_2 injection stabilizes the coal combustion. The average standard deviation of the T_{gas} and H_2O measurements for the cofiring configurations at P2 is 23 °C and 0.2% and for P4, 25 °C and 0.25%. Considering the elevated H_2O concentration in the co-fired flames, both the normalized T_{gas} and H_2O standard deviations indicate a more stable combustion during co-combustion with H_2.

There is a minor effect of burner design concept on T_{gas} and H_2O concentration. At low H_2 injection velocities (140–310 m/s) the T_{gas} close to the burner is higher than in the middle section of the furnace, with an average T_{gas} of 1416 °C measured at port 2 compared to 1312 °C at port 4, see Fig. 5e and h. While T_{gas} decreases between ports, the H_2O concentration remains constant at 5.8%, see Fig. 6e and.h, which indicates almost complete combustion already at Port 2 for low velocity burners. At high H_2 injection velocities (550–1200 m/s), the T_{gas} and

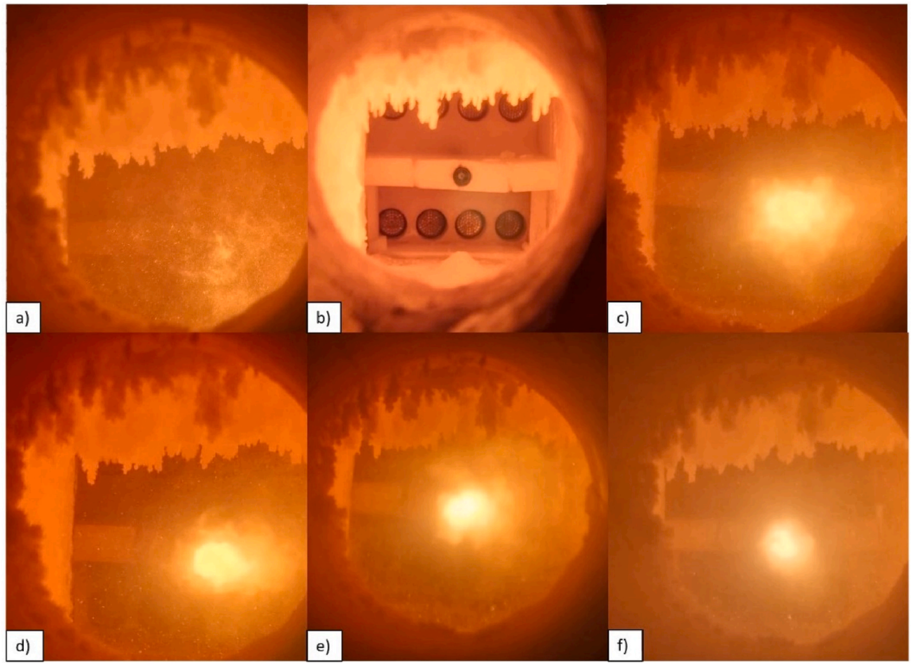

Fig. 4. Snapshots of the inside of the furnace when firing with hydrogen in the inner register. Coal combustion with burner I-A is shown in (a), H_2 combustion with burner I-A is shown in (b), and co-fired combustion are shown in (*c*–e) with burner I-A in (c), burner I–B in (d), burner I–C in (e), and burner I-D in (f).

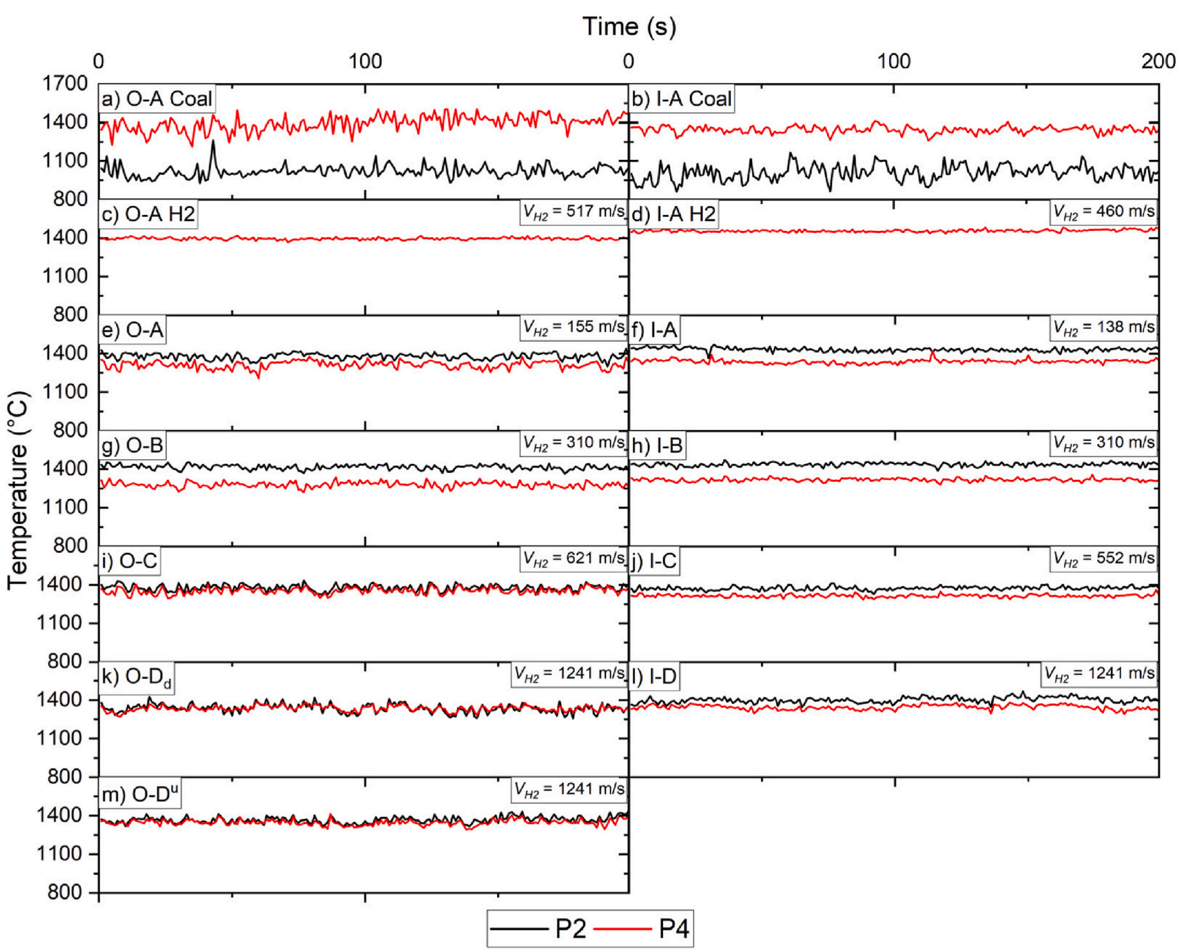

Fig. 5. Time-resolved TDLAS measurements of temperature at P2 and P4. (a) Coal combustion using the O burner. (b) Coal combustion using the I burner. (c) H_2 combustion using the O burner. (d) H_2 combustion using the I burner. (e), (g), (i), (k) and (m) corresponds to coal/H_2 cofiring with the O burner at different H_2 injection velocities. (f), (h), (j) and (l) corresponds to cofiring with the I burner at different H_2 injection velocities.

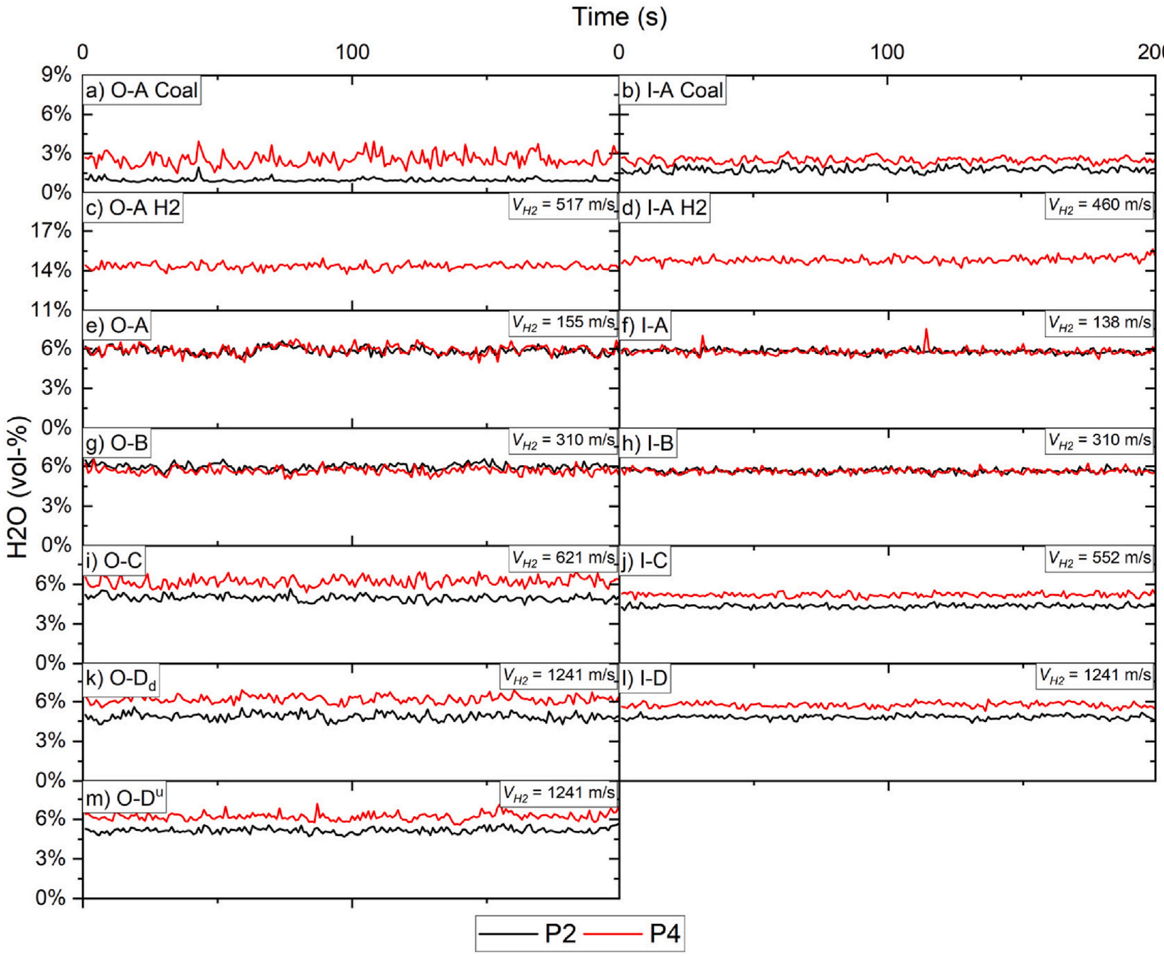

Fig. 6. Time-resolved TDLAS measurements of H_2O at P2 and P4. (a) Coal combustion using the O burner. (b) Coal combustion using the I burner. (b) H_2 combustion using the O burner. (d) H_2 combustion using the I burner. (e), (g), (i), (k) and (m) corresponds to coal/H_2 cofiring with the O burner at different H_2 injection velocities. (f), (h), (j) and (l) corresponds to cofiring with the I burner at different H_2 injection velocities.

H_2O concentration at Port 2, 1371 °C and 4.8% respectively, is decreased compared to the low velocity counterparts. At the same time, the T_{gas} at Port 4 is increased to 1339 °C with a similar H_2O concentration of 5.9% relative to the low velocity burners. The results indicate that combustion largely takes place upstream of port 2 for the low velocity burners, as the H_2O concentration remains constant between ports and there is a large decrease in T_{gas}. For the high velocity burners on the other hand, the results indicate that the flame is shifted forward by the increased momentum of the injected H_2, with combustion still ongoing between ports as suggested by the increasing H_2O concentration and a smaller drop in temperature between ports relative to the low velocity burners.

3.2. Process temperature and heat transfer

The averaged T_{proc}, T_{gas} and $T_{particle}$ or T_{wall} at the ports P2 and P4 are shown in Fig. 7. During coal combustion, the temperature in the beginning of the furnace (T_{proc}) is ~100 °C lower compared to cofiring and ~80 °C lower compared to H_2 combustion, which indicates an earlier ignition with H_2 present. Therefore, the T_{proc} profile is relatively even in the furnace for the cofiring cases. The T_{proc} at the outlet of the kiln is similar for all cases, independent of the fuel.

Due to the pulsating flame, it is possible to measure both T_{wall} and $T_{particle}$ at Port 2 by the emission spectroscopy. At P4, no (or low compared to wall radiation) coal particles are seen and only T_{wall} is measured. For all investigated cases, T_{wall} measured by the spectrometer is in good agreement with corresponding T_{proc} measured with the thermocouples. The largest difference between $T_{particle}$ and T_{gas} was measured for the pure coal flame, which is another indicator of late and varying point of ignition for this case. For the O burner concept, especially burner O-A and *O*–B, the $T_{particle}$ is 150 °C lower than that for coal combustion (1700 and 1850 °C, respectively). A reasonable explanation for this observation is that H_2O produced from the H_2 combustion interact with the combustion of the coal particle to form an oxygen deficient zone surrounding the coal jet, which reduces the maximum $T_{particle}$. Since the H_2 is injected centrally and inside the flow of the coal powder, a similar reduction could not be observed for the I burner concept.

The averaged T_{gas} increases with 350 °C between P2 and P4 for coal combustion whereas during cofiring the T_{gas} is similar or even slightly reduced between the ports - again indicating earlier ignition during cofiring. Cofiring leads to a lower T_{gas} at P4 compared to coal combustion, this can partially be explained by elevated heat losses during cofiring where the measured heat transfer is larger in port 1. The difference in ignition between pure coal and cofiring can also change the vertical location of the flame at P4 due to buoyancy effects (lifted flame flames).

The results from the total heat flux radiometer is presented in Fig. 8 and available in tabulated form in Table S5. For all cases, the total heat flux were higher at P3, compared to those at P1. During coal combustion the total heat increases from 254 kW/m^2 to 374 kW/m^2 between P1 and P3. The increase in heat transfer to the wall between P1 and P3 is not as

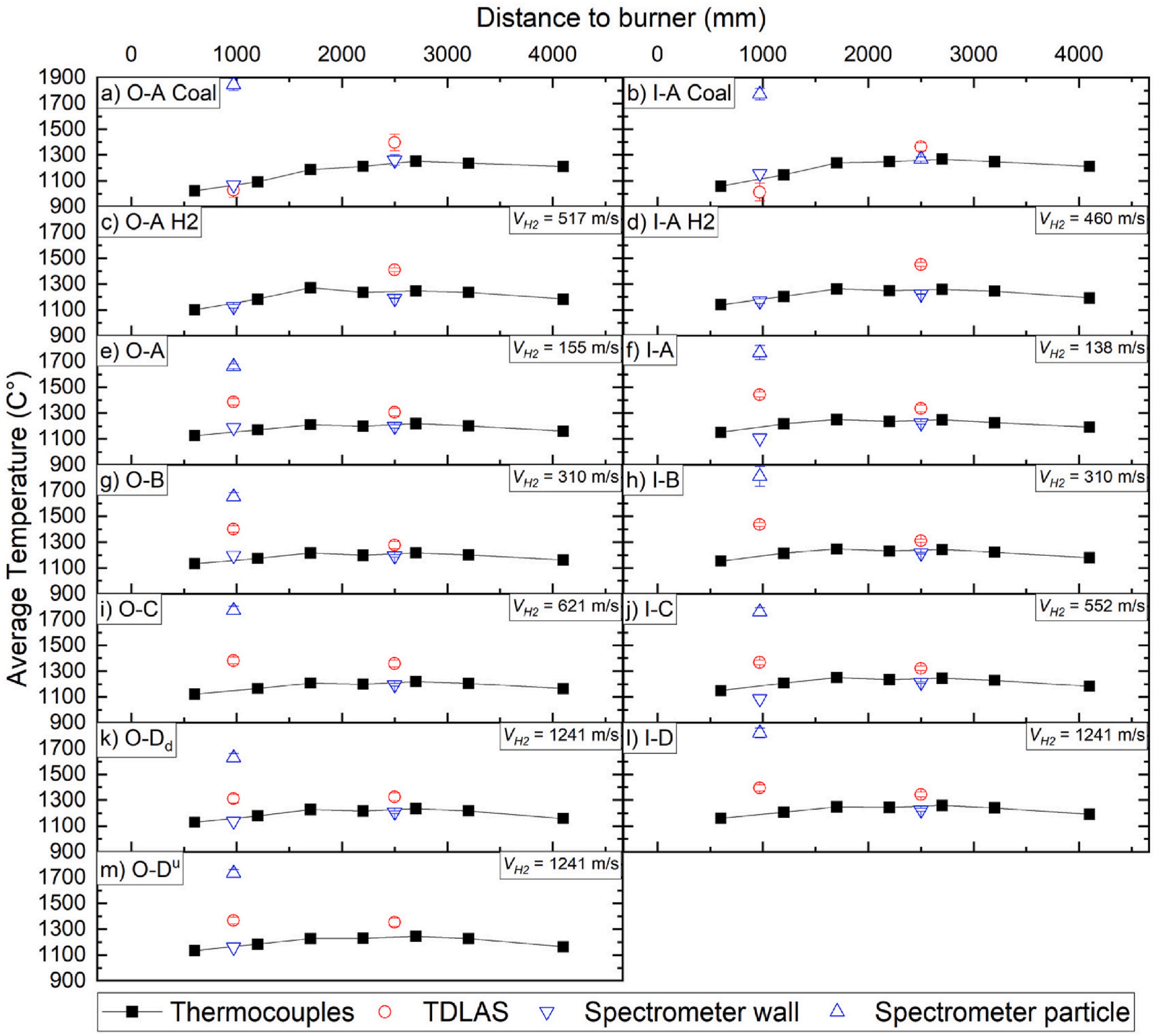

Fig. 7. Time-averaged temperature profiles measured in the furnace with the 7 thermocouples inserted through the roof of the kiln as well as the average TDLAS and spectrometer measurements in ports P2 and P4. (a) Coal combustion using the O burner. (b) Coal combustion using the I burner. (c) H_2 combustion using the O burner. (d) H_2 combustion using the I burner. (e), (g), (i), (k) and (m) corresponds to coal/H_2 cofiring with the O burner at different H_2 injection velocities. (f), (h), (j) and (l) corresponds to cofiring with the I burner at different H_2 injection velocities. Tabulated data is available in Table S3.

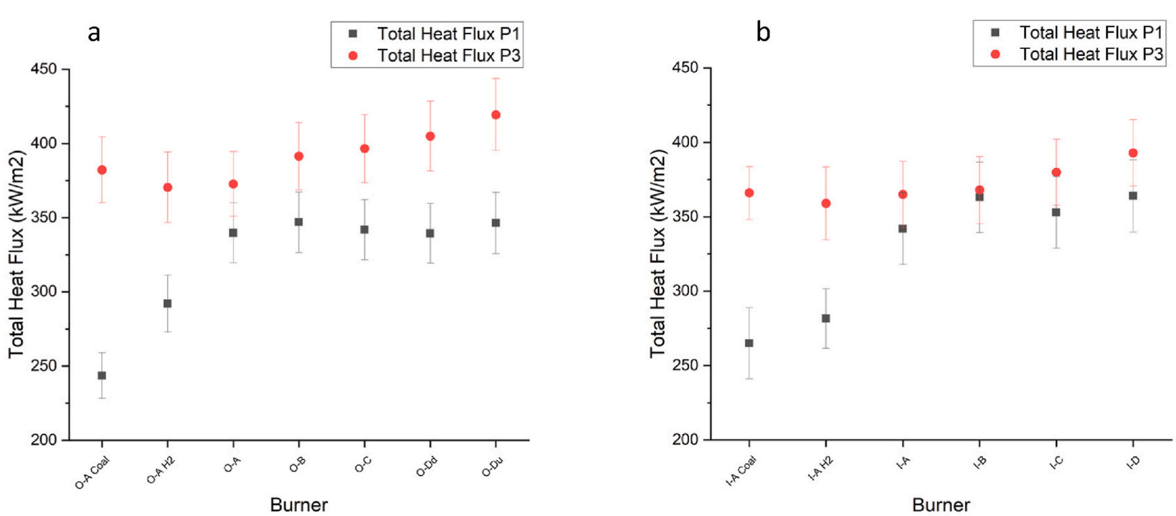

Fig. 8. Total heat flux at port P1 and port P3 measured using the total flux radiometer. (a) Corresponds to measurements using burner O and (b) corresponds to measurements using burner I.

prominent for pure H_2 and H_2/coal cofiring cases. Again, this behavior in heat transfer supports the discussion of delayed ignition and heat release for pure coal combustion compared to H_2 combustion and H_2/coal cofiring. Furthermore, cofiring results in larger total heat flux at P1 (348 kW/m^2) compared to the total heat flux (254 kW/m^2) of not only pure coal combustion, but also to pure H_2 combustion (287 kW/m^2). At P3, the total heat flux for all fuels tested are on average on similar levels. The findings in pure H_2 and pure coal combustion support recent numerical simulations by Ehlme et al. which show that H_2 flames result in higher heat transfer rates to the kiln walls close to the burner compared to coal flames [42].

The total heat flux at P3 was found to vary slightly with burner configuration when cofiring H_2 and coal. Increasing H_2 velocity results in higher total heat flux in the middle section of the furnace (P3). This is likely due to the increased turbulence intensity induced by the higher velocity H_2 jets which in turn increases the turbulence levels in the kiln downstream.

3.3. Emissions

Fig. 9 shows the measured flue gas composition (wet basis) measured at the outlet (see 7 in Fig. 1). The wet gas compositions from the FTIR and the MGA Prime instruments are presented in *Table S4*. The major gas species (O_2, H_2O, and CO_2) as well as CO show similar levels during repetitions. Furthermore, the low CO levels (<15 ppm) throughout all experiments indicate near complete combustion. The FTIR (exhaust) and TDLAS (P4) H_2O data are within the measurement accuracy for all experimental cases.

An average outlet O_2 concentration of 14.6% was measured in all cases except during H_2 combustion where the average O_2 concentration was 13.7%. The lower oxygen concentration during H_2 firing is explained by a slightly higher power: 139 kW instead of 130 kW as during coal and cofiring; note that air flow was kept constant throughout all experiments. The coal combustion resulted in 5.6% CO_2 in the flue gas on average. The carbon-free H_2 naturally resulted in zero CO_2 and cofiring resulted in an average CO_2 concentration of 3.9%. Replacing 30% of the coal during H2/coal cofiring resulted in 31% decrease in outlet CO_2.

The NO_X emissions are presented in Fig. 10 as the averaged NO_2 mass emitted per unit of energy (mg/MJ_{Fuel}), calculated from the measured outlet NO_X concentration and the flue gas flow rate estimated by assuming complete combustion. Cofiring was found to reduce NO_X emissions compared to coal combustion, with both burner concepts (O and I) resulting in similar NO_x emission levels. The average NO_x emission for the coal combustion cases was 915 mg NO_2/MJ, 2871 mg NO_2/MJ for the H_2 combustion cases, and 593 mg NO_2/MJ for the H_2/coal cofiring cases. Pure H_2 combustion produces most NO_x, due to the Zeldovich reactions associated with a high flame temperature. Cofiring H_2 and coal lead to a reduction of the NO_X formation of 35% on average compared to pure coal and a reduction of 79% compared to pure H_2 combustion. The decrease of NO_X during cofiring suggests that the (maximal) flame temperature is no longer sufficiently high to activate the substantial NO_x production due to Zeldovich mechanism once H_2 is introduced to the coal flame. This is possible provided that a significant part of the early heat release of the H_2 combustion is transferred to the coal particles. This explanation is consistent with the earlier ignition of the coal particles. The larger reduction in NO_X emission than the reduction in the mass influx of fuel-bound N in the low velocity H_2 cofiring burners O-A, *O*–B and I–C indicates the possible importance of NO reburning or char reduction pathways under the conditions studied. For example, it is well known in coal combustion that higher devolatilization temperatures yields more N release (mostly as HCN and NH_3) in the devolatilization stage [17], which can reduce NO through reactions forming N_2. The argument of early heat release of H_2 igniting the coal would also increase the devolatilization temperature of the coal particles. We plan to investigate the NO_X formation in the system during cofiring conditions numerically in our future work.

The design of the cofiring burner affected the NO_x formation by about 10%. Burners of type O generated on average 567 mg NO_2/MJ of NO_X while burners of type I generated on average 601 mg NO_2/MJ. The only burner of type O that produced more NOx than its counterpart of type I was burner O/I-D, with the highest velocity, which had a 16 mg NO_2/MJ larger formation.[1] For the other burners, H_2 injected through the outer register generated on average 51 mg/MJ less NOx compared to their counterparts with H_2 injected through the central register. No significant difference in NO_X formation was found between the two configurations of burner *O*-D, *O*-D_d and *O*-D^u. This observation is not intuitively obvious, as H_2 combustion has been shown to yield lifting flames [11], meaning that for burner *O*-D_u the hydrogen flame would lift away from the coal flame while for burner *O*-D_d it would instead lift into the coal flame. This independence of orientation could be an indication that with these burner concepts the H_2 and coal mixes well and the mixing is robust still producing a single flame.

Fig. 11 shows the NO concentration as a function of H_2 injection velocity. The NO_x formation increases almost linearly with H_2 velocity. Increased inlet velocities likely generate higher turbulence intensity in the flame. A more intense flame is known to favor NO_X formation as it reduces the residence time of the *N*-bound intermediates inside the reducing environment. The detailed effect of inlet velocity of the H_2 stream will, however, require further investigations.

4. Conclusions

In this work, co-combustion of H_2 and pulverized coal has been studied in a 150-kW furnace developed to simulate the conditions of the kiln in an iron ore grate-kiln induration machine. The fuels were fed through separate registers integrated in the same burner.

The results show that replacing 30% (energy) of the coal with H_2 results in a flame that is visually smaller, brighter and with less fluctuations regardless of burner design. The addition of H_2 stabilizes and enhances the ignition of coal particles and the combustion process. Cofiring of H_2 and coal generates the higher wall temperatures in the early part of the kiln due to an increased heat transfer compared to both pure H_2 and pure coal firing. The heat transfer in later parts of the kiln is similar for all fuels. Furthermore, the results showed that the H_2/coal cofiring generated 32% less NO_X emissions (623 mg/MJ) on average compared to coal combustion (915 mg/MJ) and 78% less than H_2 combustion (2870 mg/MJ). The decreased NO_X formation during cofiring is explained by a combination of early coal ignition, decreased amount of fuel bound nitrogen, and possibly suppression of the high flame temperatures typically found in H_2 flames due to heat transfer to the coal particles. The results indicate that the H_2 injection velocity has an impact on the NO_X emissions, with less NO_X emissions at lower H_2 velocities. The lowest H_2 injection velocity tested for each burner concept, i.e. burners O-A and I-A (155 and 138 m/s) had the lowest NO_X emissions (520 and 557 mg/MJ). The lowest NOx emissions, the low intensity flame (relative to the co-fired flames), and a more conventional coal injection design through a O-burner makes the O-A burner the most suitable for practical application. Overall, our findings support that replacing a portion of the coal with H_2 using one integrated burner in existing coal fired induration fueled rotary kilns is an attractive solution to reduce CO_2 and NO_X emissions.

CRediT authorship contribution statement

Andreas Johansson: Writing – review & editing, Writing – original draft, Visualization, Validation, Investigation, Formal analysis, Data curation, Conceptualization. **Johannes Fernberg:** Writing – review &

[1] Calculated by considering the NOx level of burner *O*-D as the average of the two orientations.

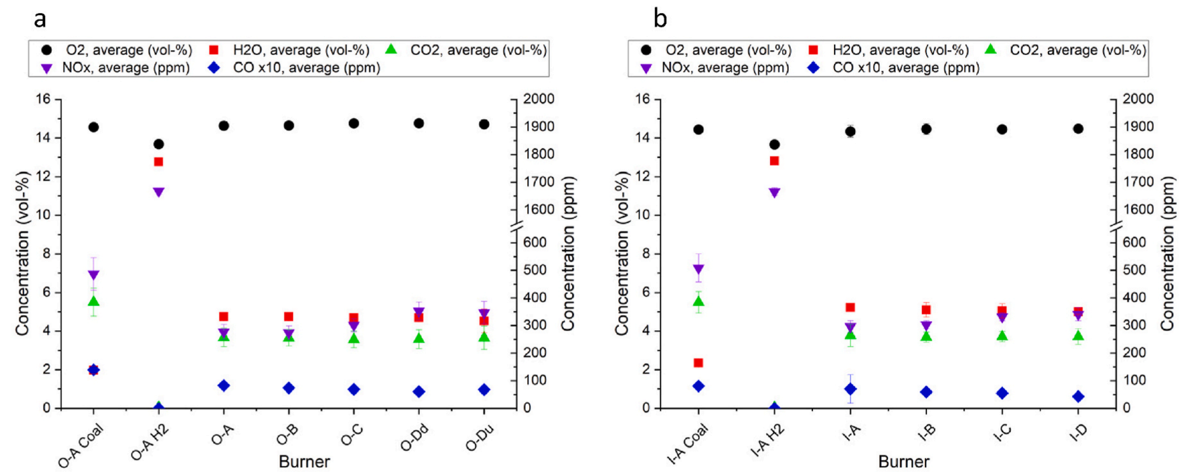

Fig. 9. Flue gas composition at the chimney using FTIR and MGA. (a) Corresponds to burner O measurements. (b) Corresponds to burner I measurements.

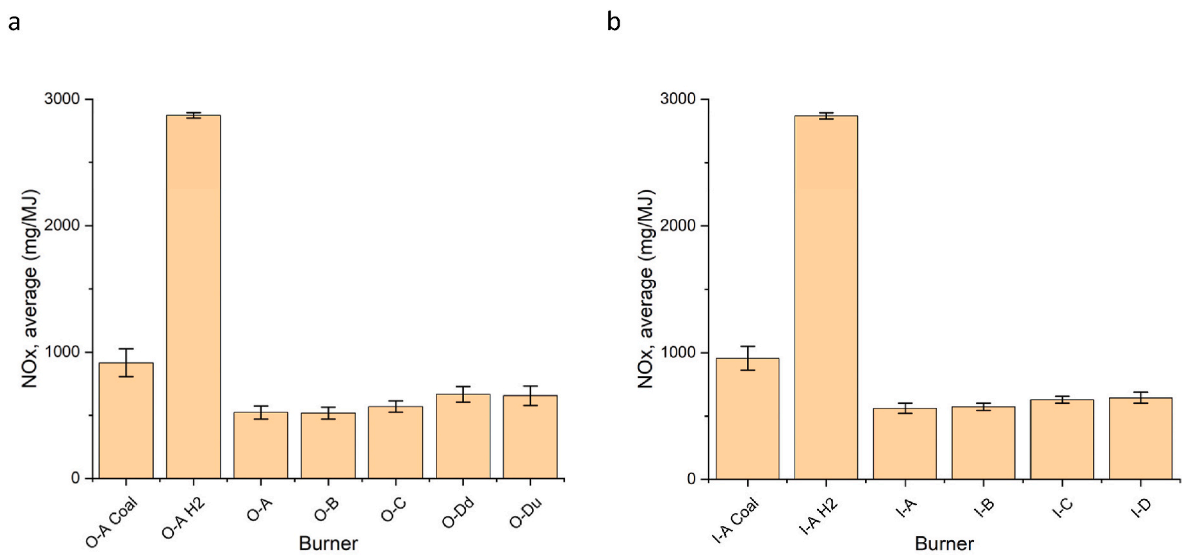

Fig. 10. Average mass of NO_X emitted at the chimney per unit of energy (a) for burner O (b) for burner I.

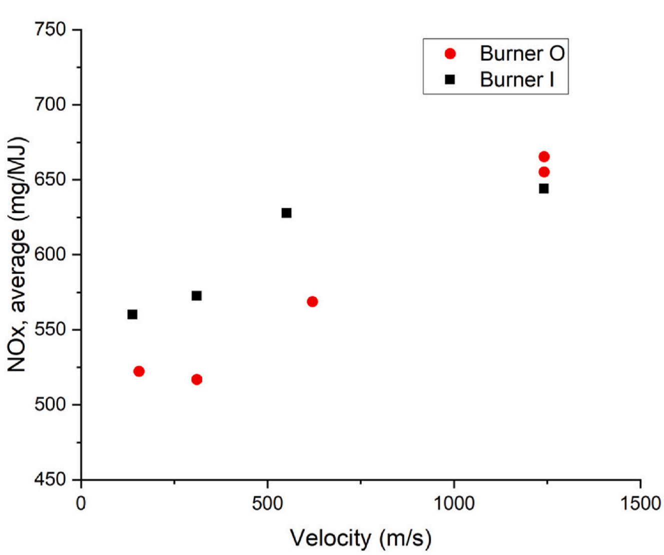

Fig. 11. Average NOx emissions of the co-fired burners as a function of H_2 injection velocity.

editing, Writing – original draft, Visualization, Validation, Methodology, Investigation, Formal analysis, Data curation, Conceptualization. **Alexey Sepman:** Writing – review & editing, Visualization, Validation, Methodology, Formal analysis, Data curation. **Samuel Colin:** Writing – review & editing. **Jonas Wennebro:** Writing – review & editing, Supervision. **Fredrik Normann:** Writing – review & editing, Project administration, Funding acquisition. **Henrik Wiinikka:** Writing – review & editing, Supervision, Project administration, Methodology, Funding acquisition, Conceptualization.

Declaration of competing interest

The authors declare that they have no known competing financial interests or personal relationships that could have appeared to influence the work reported in this paper.

Acknowledgements

The authors gratefully acknowledge Luossavaara-Kiirunavaara AB (LKAB), the Swedish Energy Agency and the European Union (EU) for the financial support of this work (P2022-00196). Additionally, all experimental support provided from our colleagues Niklas Mörtlund, Therese Vikström, Sandra Lundström and others at RISE, Piteå is greatly appreciated.

Appendix A. Supplementary data

Supplementary data to this article can be found online at https://doi.org/10.1016/j.ijhydene.2024.09.327.

References

[1] Bisulandu B, Florian H. Rotary kiln process: an overview of physical mechanisms, models and applications. Appl Therm Eng 2022;221:119637.
[2] Peray KE. The rotary cement kiln. New York: Chemical Publishing Co., Inc.; 1986.
[3] Järvensivu M, Saari K, Jämsä-Jounela S-L. Intelligent control system of an industrial lime kiln process. Control Eng Pract 2001:589–606.
[4] Fan X-h, Li J, Chen X-l, Wang Y, Gan M. Temperature field simulation model for rotary kiln of iron ore oxidised pellet. J Iron Steel Res Int 2012;20(4):16–9.
[5] Ernst W, Lynn P, Nathan M, Chris H, Leticia OM. Carbon dioxide emissions from the cement industry. Annu Rev Environ Resour 2001;26:303–29.
[6] Vogl V, Åhman M, Nilsson LJ. Assessment of hydrogen direct reduction for fossil-free steelmaking. J Clean Prod 2018;203:736–45.
[7] Koolen D, Vidovic D. Greenhouse gas intensities of the EU steel industry and its trading partners. Luxembourg: Publications Office of the European Union; 2022.
[8] UNFCCC. Paris agreement to the united nations framework convention on climate change. 2015. p. 16–1104.
[9] European Commision. Regulation (EU) 2021/1119: European climate law. 2021.
[10] Julian S. Technologies to decarbonise the EU steel industry. Publications Office of the European Union; 2022.
[11] Wiinikka H, Sepman A, Ögren Y, Lindblom B, Nordin L-O. Combustion evaluation of renewable fuels for iron-ore pellet induration. Energy Fuel 2019:7819–29.
[12] Edland R, Smith N, Allgurén T, Fredriksson C, Normann F, Haycock D, Johnson C, Frandsen J, Fletcher TH, Andersson K. Evaluation of NOx-reduction measures for iron-ore rotary kilns. Energy Fuel 2020;34(4):4934–48.
[13] Seinfield JH, Pandis SN. Atmospheric chemistry and physics. first ed. New York: Wiley-VCH; 1986.
[14] Glaude P-A, Fournet R, Bounaceur R, Molière M. Adiabatic flame temperature from biofuels and fossil fuels and derived effect on NOx emissions. Fuel Process Technol 2010;91(2):229–35.
[15] Pitz RW, Cattolicat R, Robben F, Talbot L. Temperature and density in a hydrogen-air flame from Rayleigh scattering. Combust Flame 1976;27:313–20.
[16] Zeldovich J. The oxidation of nitrogen in combustion and explosions. Eur Phys J A 1946;21:577–628.
[17] Edland R. NOx Formation in Iron Ore Rotary Kilns for Iron ore Pelletization. Gothenburg: Chalmers University of Technology; 2019. Lic. Thesis.
[18] Gunnarsson A. Radiative heat transfer in suspension-fired Systems. Gothenburg: Chalmers Univerity of Tehnology; 2019. Phd. Thesis.
[19] Correa SM. A review of NOx formation under gas-turbine combustion conditions. Combust Sci Technol 1991;87(1–6):329–62.
[20] Kurosea R, Makinob H, Suzukic A. Numerical analysis of pulverized coal combustion characteristics. Fuel 2003;83(6):693–703.
[21] Pisa I, Lazaroiu G, Prisecaru T. Influence of hydrogen enriched gas injection upon polluting emissions from pulverized coal combustion. Int J Hydrogen Energy 2014; 39(31):17702–9.
[22] Hercog J, Lewtak R, Glot B, Jóźwiak P, Nehring G, Domingos V, Tavares AMN, Gaspar D. Pilot testing and numerical simulations of the multifuel burner for the cement kiln. Fuel 2023;342:127801.
[23] Liu Y, Hu Z, Shen Y. CFD study of hydrogen injection in blast furnaces. Metall Mater Trans B 2021;52(5):2971–91.
[24] Ueki Y, Yoshiie R, Naruse I, Matsuzaki S. Effect of hydrogen gas addition on combustion characteristics of pulverized coal. Fuel Process Technol 2017;161: 289–94.
[25] Mustafa Ilbas SK. A numerical study on combustion behaviours of hydrogen-enriched low calorific value coal gases. Int J Hydrogen Energy 2015;40(44): 15218–26.
[26] Kim K-M, Kim G-B, Lee B-H, Jeon C-H, Keum J-H. Methane gas cofiring effects on combustion and NOx emission in 550 MW tangentially fired pulverized-coal boiler. ACS Omega 2021;6(46):31132–46.
[27] Aoyang Z, Xiaowei L, Yishu X, Yunfei Z, Yuyang L, Minghou X. Effect of ammonia and coal co-firing on the formation mechanism and composition characteristics of particulate matter. Fuel 2024;358:130231.
[28] Xian D, Wangfan L, Pingyuan L, Zhizhong K. Numerical calculation on combustion process and NO transformation behavior in a coal-fired boiler blended ammonia: effects of the injection position and blending ratio. Int J Hydrogen Energy 2023;48: 29771–85.
[29] Valera-Medina A, Vigueras-Zuniga MO, Shi H, Mashruk S, Alnajideen M, Alnasif A, Davies J, Wang Y, Zhu X, Yang W, Cheng YB. Ammonia combustion in furnaces: a review. Int J Hydrogen Energy 2024;49:1597–618.
[30] Chen P, Cheng G, Changhao H, Mingyan G, Boyu J, Jianren F. Mechanism analysis of fuel-N oxidation during ammonia-coal co-combustion: influence of H2O. Fuel 2023;342:127747.
[31] Sakiko I, Juwei Z, Takamasa I. Numerical calculation with detailed chemistry on ammonia co-firing in a coal-fired boiler: effect of ammonia co-firing ratio on NO emissions. Fuel 2020;274:117742.
[32] Tamura M, Gotou T, Ishii H, Riechelmann D. Experimental investigation of ammonia combustion in a bench scale 1.2MW-thermal pulverised coal firing furnace. Appl Energy 2020;277:115580.
[33] Science and technology of ammonia combustion. Proc Combust Inst 2019;37(1): 109–33.
[34] Nordgren S. Energy analysis of pelletising in a straight grate induration furnace. Lic. Thesis. Luleå: Luleå University of Technology; 2010.
[35] Chedaille J, Braud Y. Measurements in Flames. London: Edward Arnold; 1972.
[36] Ögren Y, Gullberg M, Wennebro J, Sepman A, Toth P, Wiinikka H. Influence of oxidizer injection angle on the entrained flow gasification of torrified wood powder. Fuel Process Technol 2018;181:8–17.
[37] Sepman A, Ögren Y, Wennebro J, Wiinikka H. Simultaneous diagnostics of fuel moisture content and equivalence ratio during combustion of liquid and solid fuels. Appl Energy 2022;324:119731.
[38] Sepman A, Fredriksson C, Ögren Y, Wiinikka H. Laser-based, optical, and traditional diagnostics of NO and temperature in 400 kW pilot-scale furnace. Appl Sci 2021;11(15):7048.
[39] Matsugi A. Exploring the mechanism of blue emission from hydrogen combustion. Combust Flame 2023;256:112953.
[40] Bayless DJ, Schroeder AR, Johnson DC, Peters JE, Krier H, Buckius RO. The effects of natural gas cofiring on the ignition delay of pulverized coal and coke particles. Combust Sci Technol 1994;98(1–3):185–98.
[41] Qu Z, Schmidt F. In situ H2O and temperature detection close to burning biomass pellets using calibration-free wavelength modulation spectroscopy. Appl Phys B 2015;119(1):45–53.
[42] Ehlme E, Gunnarsson A, Andersson K, Normann F. Heat transfer conditions in hydrogen-fired rotary kilns for iron ore processing. Ind Eng Chem Res 2023;62(37): 15098–108.